

RESEARCH ARTICLE

10.1002/2014JD021621

Key Points:

- SSWs impact polar motion and length-of-day variations

Supporting Information:

- Readme
- Figure S1
- Figure S2
- Figure S3

Correspondence to:

L. Neef,
lneef@geomar.de

Citation:

Neef, L., S. Walther, K. Matthes, and K. Kodera (2014), Observations of stratospheric sudden warmings in Earth rotation variations, *J. Geophys. Res. Atmos.*, 119, 9666–9678, doi:10.1002/2014JD021621.

Received 10 FEB 2014

Accepted 29 JUL 2014

Accepted article online 4 AUG 2014

Published online 19 AUG 2014

Observations of stratospheric sudden warmings in Earth rotation variations

Lisa Neef¹, Sophia Walther², Katja Matthes¹, and Kunihiko Kodera³

¹Ocean Circulation and Climate Dynamics - Marine Meteorology, Helmholtz Centre for Ocean Research Kiel (GEOMAR), Kiel, Germany, ²Institute for Meteorology, Free University of Berlin, Berlin, Germany, ³Solar-Terrestrial Environment Laboratory, Nagoya University, Nagoya, Japan

Abstract Stratospheric sudden warmings (SSWs) are extreme events in the polar stratosphere that are both caused by and have effects on the tropospheric flow. This means that SSWs are associated with changes in the angular momentum of the atmosphere, both before and after their onset. Because these angular momentum changes are transferred to the solid Earth, they can be observed in the rate of the Earth's rotation and the wobble of its rotational pole. By comparing observed Earth rotation variations to reanalysis data, we find that an anomaly in the orientation of the Earth's rotational pole, up to 4 times as large as the annual polar wobble, typically precedes SSWs by 20–40 days. The polar motion signal is due to pressure anomalies that are typically seen before SSW events and represents a new type of observable that may aid in the prediction of SSWs. A decline in the length of day is also seen, on average, near the time of the SSW wind reversal and is found to be due to anomalous easterly winds generated in the tropical troposphere around this time, though the structure and timing of this signal seems to vary widely from event to event.

1. Introduction

Stratospheric sudden warmings (SSWs) are extreme events that happen roughly every other year in the polar stratosphere; the usually cold polar vortex warms up (usually 30°–50°C) over the course of a few days, and the vortex winds reverse from westerly to easterly. Figure 1 shows the (a) temperature and (b) zonal wind anomalies over the polar cap during the warming event of January 2009, which was exceptionally strong and unexpected [Harada *et al.*, 2009; Ayarzagüena *et al.*, 2011]. The reversal of zonal wind at 60°N propagated downward in time, crossing the 10 hPa surface on 24 January 2009; this date is defined by Charlton and Polvani [2007] as the *central date* of the warming.

The 2009 SSW was the result of strong tropospheric forcing, in the form of a Rossby wave packet that was excited by a deep ridge over the eastern Pacific region, and a cyclonic anomaly in the North Atlantic region [Ayarzagüena *et al.*, 2011]. It not only affected tropospheric weather but also the rotation of the Earth. Figures 1c and 1d show observations of three parameters of Earth rotation over the course of the 2009 SSW. The first two parameters, χ_1 and χ_2 , are angles that define the motion of the Earth's rotational pole (after rotating to a terrestrial reference frame; see section 2.1), and the third is the deviation in the length of a day from its 24 h period. In all three parameters, we have removed the daily climatology (in order to remove the seasonal cycle) as well as the 151 day average around the central date (in order to remove inter-annual variability due to, e.g., the quasi-biennial oscillation or El Niño–Southern Oscillation (ENSO)). This leaves the subseasonal fluctuations, which are typically on the order of tens of milliarseconds for the polar motion angles, and microseconds for the length-of-day anomalies [Salstein and Rosen, 1989; Eubanks *et al.*, 1985; Rosen *et al.*, 1991]. Polar motion angle 2 in particular shows a negative anomaly of 30 mas about 3 weeks before the central date, while the length-of-day anomaly shows a steady decline as the central date is approached and passed. But are these features related to the SSW, and if so, why?

Earth rotation parameters may be unusual observables for studying SSWs, but can actually serve as a global measure of atmospheric dynamics because they reflect the atmosphere's angular momentum (AAM). Angular momentum within the Earth system is conserved in the absence of outside torques; therefore, changes in the axial AAM change the Earth's rotational velocity, and changes in the two equatorial components of AAM change the orientation of the Earth's rotational pole. Of course there are also other sources of angular momentum in the Earth system (the ocean, continental hydrosphere, and solid Earth), but on

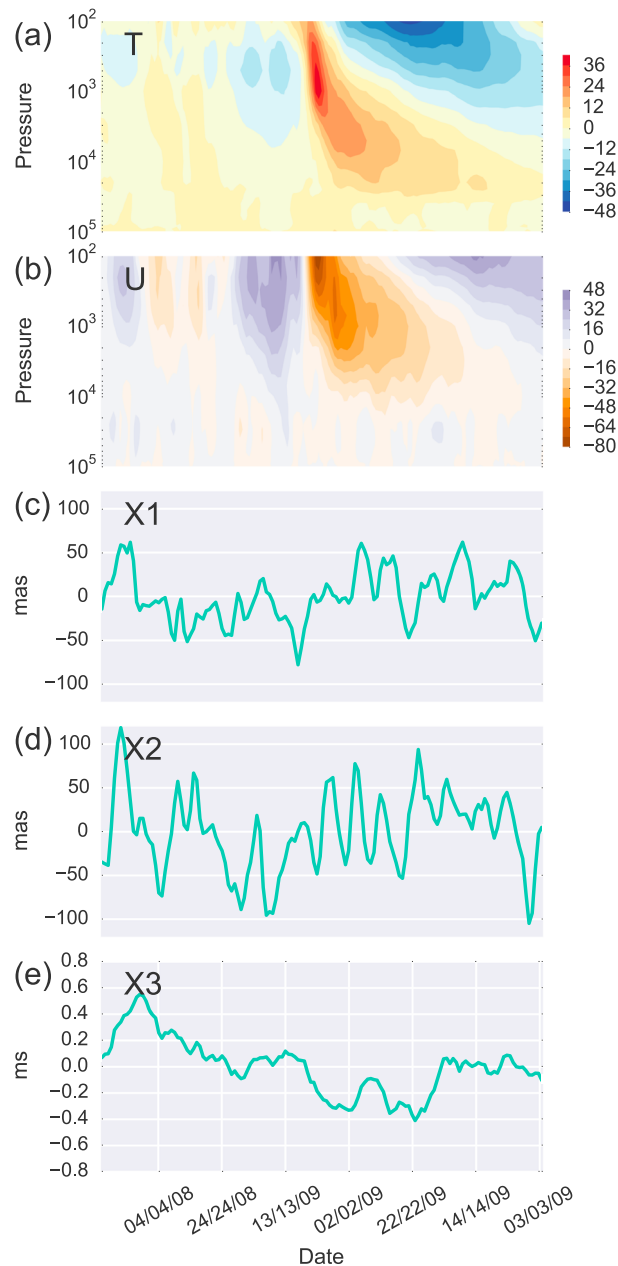


Figure 1. (a, b) Altitude-time composites of the polar cap (60°–90°N) temperature and 60°N zonal wind anomalies for the January 2009 SSW event. (c–e) The observed anomalies in the three Earth rotation parameters over the same time.

anomalous global meridional circulation that causes upwelling in the tropics, cooling of the tropical lower stratosphere, and consequently a westerly wind anomaly in the north subtropical stratosphere [Kodera, 2006] and increased convection in the southern tropics [Kodera et al., 2011].

Thus, it is likely that SSWs might alter the global AAM. In order to identify the footprint of SSWs in the record of observed Earth rotation variations we have composited observations of polar motion and length-of-day variations over the known SSW events in the 48 years since the beginning of the modern Earth rotation record (1962–2010), and compared these composites to the corresponding atmospheric excitation of Earth rotation variations, as implied by reanalysis data.

The paper is organized as follows. Section 2 outlines the observational and reanalysis data used, and the connection between observed Earth rotation variations and geophysically modeled AAM excitation

subseasonal time scales the atmosphere is the dominant source of axial angular momentum [Rosen and Salstein, 1983; Eubanks et al., 1985] and a major source, along with the ocean, of equatorial angular momentum [Dobslaw et al., 2010].

Total AAM is the sum of the relative angular momentum of the atmosphere (i.e., winds) and changes in the atmospheric moment of inertia (i.e., the atmospheric mass distribution). For example, the seasonal variation in the extratropical tropospheric jets causes a change in the axial relative AAM, which causes the length of day to fluctuate by about 1 ms every year [Hide et al., 1997]. Likewise, the annual appearance of the Siberian high-pressure system causes a yearly fluctuation in the two equatorial components of AAM, which results in a polar wobble of several mas [Chao and Au, 1991; Nastula et al., 2009; Dobslaw et al., 2010].

In this paper we ask the question of whether SSWs affect AAM and, by extension, the rotation of the Earth. The effect of stratospheric phenomena on Earth rotation variations has not been studied much, primarily because the low mass of the stratosphere typically makes its contribution to total AAM quite small [Rosen and Salstein, 1985; Zhou et al., 2008]. However, SSWs are a stratospheric phenomenon with strong links to the troposphere; not only do they affect tropospheric weather for 1–2 months after the start of the warming [Baldwin and Dunkerton, 2001; Thompson et al., 2002; Woollings et al., 2010], but they are also, typically, preceded by large-scale midlatitude and high-latitude pressure anomalies that trigger or enhance upward propagating planetary waves [Quiroz, 1986; Martius et al., 2009; Woollings et al., 2010; Garfinkel et al., 2010; Ayarzagüena et al., 2011]. Moreover, it has been shown that SSWs induce an

functions. The observed Earth rotation variations during SSWs are summarized in section 2.1. Then section 4 examines the impact of SSWs on polar motion, while section 5 examines the impact of major SSWs on the rate of Earth's rotation. A discussion and conclusions are given in section 6.

2. Methods

2.1. Earth Rotation Observations

Earth rotation variations are described by anomalies in the length of day and the orientation of the Earth's figure axis. These so-called Earth rotation parameters (ERPs hereafter) are observed by a combination of optical astrometry, lunar and satellite laser ranging, Very Long Baseline Interferometry, and GPS, and are compiled regularly by the International Earth Rotation and Reference Systems Service. We have used the ERP series number C04-08, which contains daily measurements over the period 1962 to the present day and is available online at <http://hpiers.obspm.fr/eop-pc/>. In this data set, solid Earth tides (ranging in period from 5.64 days to 18.6 years) have been removed in postprocessing, while semidiurnal and diurnal ocean tide signals fall away due to the daily resolution of the data.

The angles of polar motion, p_1 and p_2 , represent the location of the Earth's rotational axis in an inertial, celestial reference frame that is fixed in space and defined relative to a group of stars (the so-called celestial ephemeris pole). *Barnes et al.* [1983] and later *Gross* [1992] showed that these vectors can be directly related to unit variations in the equatorial components of the Earth's angular momentum, χ_1 and χ_2 (defined along the Greenwich meridian and the 90°E meridian, respectively) using the following:

$$p_1 + \frac{\dot{p}_2}{\sigma_0} = \chi_1^{\text{GEO}} \quad (1)$$

$$-p_2 + \frac{\dot{p}_1}{\sigma_0} = \chi_2^{\text{GEO}}, \quad (2)$$

where the overdots represent time derivatives and "GEO" denotes that the angular momentum components are observed geodetically rather than derived from mechanical equations. Note that this equation involves a rotation into an inertial reference frame of the so-called Chandler wobble, a free nutation of the Earth of frequency $\sigma_0 = 2\pi/433\text{d}$, which results from the oblateness of the Earth's figure.

The third ERP is ΔLOD , i.e. the difference between the duration of the day that is determined astronomically and the solar day. It is simply related to unit changes in the axial component of angular momentum, χ_3 :

$$\frac{\Delta\text{LOD}}{\text{LOD}_0} = \Delta\chi_3, \quad (3)$$

where LOD_0 represents the nominal length of day, 86,400 s.

Since the introduction of satellite geodesy in the early 1980s, the accuracy of the polar motion data has improved from about 30 mas to about 30 μas , while the accuracy of the LOD anomalies has improved from about 1.5 ms to about 15 μs .

2.2. Atmospheric Excitation Functions

The angular momentum excitation functions χ_i ($i = 1, 2, 3$) actually represent the net angular momentum of the entire Earth system, including the atmosphere, oceans, continental hydrosphere, and solid Earth. On time scales from a few days to months, fluctuations in the angular momentum of the atmosphere, modified by the response of the sea levels to pressure loading from the atmosphere [*Eubanks et al.*, 1988], dominate changes in both LOD [*Rosen and Salstein*, 1983; *Rosen et al.*, 1990] and polar motion. The rest of this manuscript will examine only the atmospheric angular momentum excitation functions (AEFs hereafter), with the exception of some oceanic effects covered in section 4.1.

Each AEF can be separated into contributions from relative angular momentum (hereafter the wind term, χ_i^{W}) and changes in the atmospheric moment of inertia (hereafter the mass term, χ_i^{M}). The wind and mass

terms are as follows [Barnes *et al.*, 1983]:

$$\chi_1^M = \frac{-1.10R^4}{(g(C-A))} \int \int p_s \sin \phi \cos^2 \phi \cos \lambda d\lambda d\phi \quad (4)$$

$$\chi_1^W = \frac{-1.61R^3}{\Omega(C-A)g} \int \int \int (u \sin \phi \cos \phi \cos \lambda - v \cos \phi \sin \lambda) d\lambda d\phi dp \quad (5)$$

$$\chi_2^M = \frac{-1.10R^4}{(g(C-A))} \int \int p_s \sin \phi \cos^2 \phi \sin \lambda d\lambda d\phi \quad (6)$$

$$\chi_2^W = \frac{-1.61R^3}{\Omega(C-A)g} \int \int \int (u \sin \phi \cos \phi \sin \lambda + v \cos \phi \cos \lambda) d\lambda d\phi dp \quad (7)$$

$$\chi_3^M = \frac{0.748R^4}{C_m g} \int \int p_s \cos^3 \phi d\lambda d\phi \quad (8)$$

$$\chi_3^W = \frac{0.997R^3}{C_m \Omega g} \int \int \int u \cos^2 \phi d\lambda d\phi dp, \quad (9)$$

where ϕ and λ represent latitude and longitude, respectively, p_s represents the surface pressure, and u and v are the zonal and meridional winds, respectively. $R = 6371.0$ km represents the radius of the Earth, $\Omega = 7.292115 \times 10^{-5}$ rad/s the average rotation rate, and $g = 9.81$ m/s² the acceleration due to gravity. $C = 8.0365 \times 10^{37}$ kg m² and $A = 8.0101 \times 10^{37}$ kg m² are the axial and next-largest principal moments of inertia of the solid Earth, and $C_m = 7.1236 \times 10^{37}$ kg m² is the principal inertia tensor component of the Earth's mantle [Gross, 2009].

Note that the equatorial excitation functions χ_1 and χ_2 are actually defined in radians, while the axial excitation function χ_3 is dimensionless. The trigonometric functions that weight wind and surface pressure in each integral come from the reference frame in which the ERPs are defined and are illustrated graphically in supporting information Figures S1–S2.

It is also worth noting that χ_3 , which excites Δ LOD, depends only on zonal wind and surface pressure and is weighted most strongly in the tropics, with uniform zonal weighting. In contrast, the equatorial excitation functions χ_1 and χ_2 also depend on the meridional wind and are weighted most strongly at midlatitudes, with a wave 1 zonal weighting (see supporting information). Note also that the wind excitation functions ((5), (7), and (9)) involve integrals over the mass of the atmosphere and are therefore weighted the most at the lowest levels, where the mass is highest.

2.3. Reanalysis Data

SSWs are examined using the two major reanalyses of the European Centre for Medium-Range Weather Forecasts (ECMWF), ERA-40 [Uppala *et al.*, 2005], and ERA-Interim [Dee *et al.*, 2011], both at 2.5° horizontal resolution. These data are freely available online at <http://data-portal.ecmwf.int/>. Only ERA-Interim data (1979–2010) were used for the polar motion analysis in section 4, because this analysis relies heavily on surface pressure data, whereas only sea level pressure is publicly available in the ERA-40 reanalysis. For the analysis of Δ LOD (section 5), which focuses on wind excitation, the two data sets were selected for the vertical levels that they have in common, with the top at 1 hPa, and joined together at 1 April 1979; this uses as many ERA-Interim data as possible while keeping the junction away from the major warming event of February 1979.

2.4. Selection of Major Warming Events

SSWs are generally defined by rapidly increasing temperatures in the stratospheric polar vortex, along with an abrupt reversal of the vortex winds. Major midwinter warmings are defined by the World Meteorological Organization as events where the zonal mean zonal wind at 10 hPa and 60°N becomes easterly during boreal winter (November–March) and where simultaneously the meridional gradient in zonal mean temperature at 10 hPa and 60–85°N is positive for more than 5 days [Labitzke and Naujokat, 2000].

In this study, major warming events are identified following the method of Charlton and Polvani [2007], which identifies SSWs by the wind criterion of the WMO definition. The first day where the wind at 10 hPa and 60°N reverses to easterly is defined as the central date of the warming. In order to ensure that events with small westerly wind fluctuations are not counted twice, no day within 20 days of this central date can also be defined as a central date. Final warmings, i.e., warmings where the vortex does not recover before the onset of the easterly summer circulation, are excluded from our analysis. This procedure is also done

Table 1. Major Stratospheric Sudden Warming Events Identified in ERA-40 (1958–1978) and ERA-Interim (1979–2010)

ERA-40	ERA-Interim
31 Jan 1958 ^a	29 Feb 1980 ^b
15 Jan 1960 ^{a,b}	4 Mar 1981
28 Jan 1963	4 Dec 1981 ^b
16 Dec 1965 ^c	24 Feb 1984 ^b
23 Feb 1966	1 Jan 1985
7 Jan 1968	23 Jan 1987
28 Nov 1968	8 Dec 1987
13 Mar 1969	14 Mar 1988 ^d
2 Jan 1970	21 Feb 1989
18 Jan 1971	15 Dec 1998
20 Mar 1971	26 Feb 1999
31 Jan 1973	20 Mar 2000 ^b
9 Jan 1977	11 Feb 2001
22 Feb 1979 ^d	30 Dec 2001
	18 Jan 2003
	5 Jan 2004
	21 Jan 2006
	24 Feb 2007
	22 Feb 2008
	24 Jan 2009
	9 Feb 2010
	24 Mar 2010

^aWarmings that are excluded because they fall outside of the ERP observation record.

^bWarmings that are not found in the observational record of *Labitzke and Naujokat* [2009].

^cWarmings that are identified as Canadian Warmings (i.e., warmings where the anomalous warm temperatures are observed mainly in the lower stratosphere) in the observational record of *Labitzke and Naujokat* [2009].

^dWarmings that are identified as final in the observational record of *Labitzke and Naujokat* [2009].

following *Charlton and Polvani* [2007] by requiring that winds must return to winter (westerly) wind conditions for at least 10 consecutive days before 30 April for an event to be considered nonfinal.

The above approach results in 14 major warmings identified in the ERA-40 period (1957–1979) and 22 events in the ERA-Interim period (1980–2010). These events are listed, in order of their central dates, in Table 1. Only the period of overlap between the reanalysis data and the ERP observations (1962 to the present day) can be used; thus, the SSWs of 1958 and 1960 are excluded. This leaves a total of 34 major SSWs on which to perform our analysis.

The events shown in Table 1 are in general agreement with the long-term meteorological observations performed at the Free University of Berlin (FUB) (*Labitzke and Naujokat* [2000] and online at <http://www.geo.fu-berlin.de/met/ag/strat/produkte/northpole/index.html>), with the exception of seven events identified as major warmings in this study but not by the FUB record (see Table 1 caption). These seven events also qualify as major warmings in the studies of *Charlton and Polvani* [2007] (which used the NCEP/NCAR reanalysis set) and *Bancalá et al.* [2012] (which used ERA-40 data exclusively) but are generally weaker events without a strong tropospheric effect.

The events shown in Table 1 represent instances where the stratospheric and possibly tropospheric flow was significantly disturbed. Could these events also have influenced Earth rotation, as in the 2009 event (Figure 1)? In order to answer this question, it is necessary to compute the AAM during these events; this will be discussed in the next section.

3. Observed Earth Rotation Anomalies During SSWs

Figure 2 is similar to Figure 1, but here the wind, temperature, and ERP anomalies have all been composited over the 34 major warming events identified in the combined ERA data set, from 1962 to 2010. The composites in each panel are centered on the central date of each event. For the three ERP observations (Figures 2c–2e), the 96% confidence interval has been estimated using a stationary bootstrap algorithm [*Wilks*, 1995] and is shown by shading.

Figures 2a and 2b illustrate the overall patterns common to major warmings, namely, that the positive temperature anomalies start in the upper stratosphere several days before the central date, preceding the reversal in zonal wind, and that both the temperature and wind anomalies propagate downward into the lower stratosphere, lasting about 40–60 days after the central date.

Figures 2c–2e show the observed ERPs, again rotating the polar motion angles to their respective angular momentum components and now also compositing over the 34 SSW events. As in Figure 1, we have removed the 151 day mean around the central date for each rotation parameter. A statistically significant signal can be seen in χ_2 and (for a few days around the central date) in ΔLOD , both parameters showing qualitatively the same behavior that was seen in the 2009 event (Figure 1): χ_2^{GEO} swings from positive to negative anomalies over the 2 months preceding the central date and then takes on weak positive anomalies after the central date, while ΔLOD declines rapidly in the 2 weeks before the central date and then recovers slowly toward zero anomalies over the 50 or so days after the central date. It is worth mentioning that this result is also found when compositing separately over the events that fall into the presatellite era (circa 1962–1981) and events in the satellite era (1981 forward).

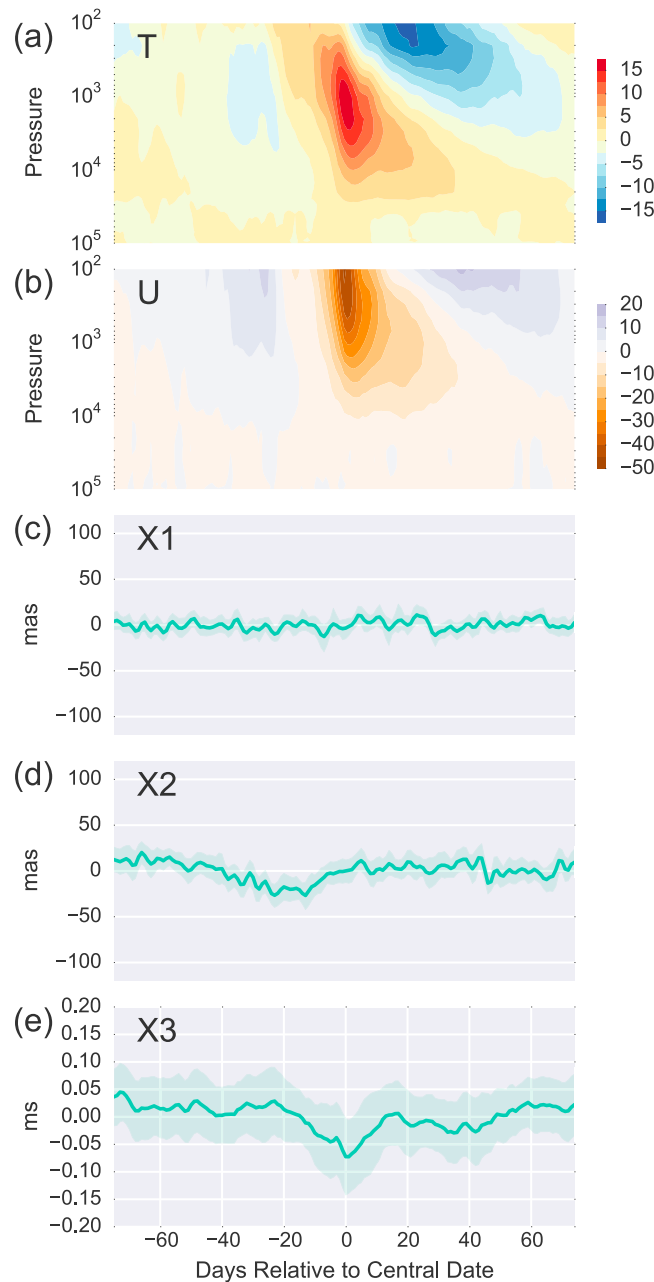


Figure 2. (a, b) Altitude-time composites of the polar cap (60°–90°N) temperature and 60°N zonal wind anomalies, composited over the SSW events given in Table 1 and centered on the central date. (c–d) The observed anomalies in the three Earth rotation parameters composited over the same events. The shading in ERP composites indicates the 96% bootstrap confidence interval.

able in ERA-40, the curves in Figure 3 are composites over only the 22 SSWs in ERA-Interim. The blue lines show the pure mass excitation functions computed from (4) and (6). Both χ_1^M and χ_2^M show large fluctuations over the SSW life cycle, but for the observations, only χ_2^{GEO} shows strong observed polar motion variations.

The difference between the large fluctuation seen in χ_2^{GEO} and the weak fluctuation seen in χ_1^{GEO} is explained when the AAM excitation functions are adjusted for the response of the oceans to atmospheric mass loading. This response can be simply modeled by averaging the surface pressure over the oceans globally, the so-called “inverted barometer” approximation [Wunsch and Stammer, 1997]. The adjusted excitation

4. Polar Motion Excitation by Mass Anomalies During SSWs

Figure 1(d) shows that the 2009 SSW was preceded by negative anomalies in χ_2^{GEO} , the atmospheric angular momentum component defined along the Greenwich meridian. This signal can also be seen in the composite over all 34 SSW events, while no clear signal was seen in the other component, χ_1^{GEO} .

The polar motion AEFs ((4)–(7)) are weighted zonally following sine and cosine waves, which means that only zonally asymmetric wind and mass anomalies result in a net polar motion excitation. Consequently, subseasonal variations in polar motion are not generally excited by wind anomalies, which tend to cancel out in the zonal integral [Barnes et al., 1983; Eubanks et al., 1988], but rather by midlatitude anomalies in the atmospheric mass distribution. Mass anomalies in the middle troposphere are a common precursor of SSWs, because they excite upward propagating planetary waves that break and thereby weaken the vortex, and SSWs are often preceded by persistent northern European blocking anticyclones [Quiroz, 1986; Martius et al., 2009; Woollings et al., 2010] and positively correlated to warm ENSO events [Garfinkel and Hartmann, 2008]. The impact of these mass variations on polar motion is investigated in the following two subsections.

4.1. Inverted Barometer Response of the Ocean

Figure 3 compares the observed equatorial AAM components with their corresponding mass excitation functions χ_1^M and χ_2^M ((4) and (6)), over 75 days on either side of the central date. Because the excitation functions ((4) and (6)) are integrals of surface pressure, which is not publicly avail-

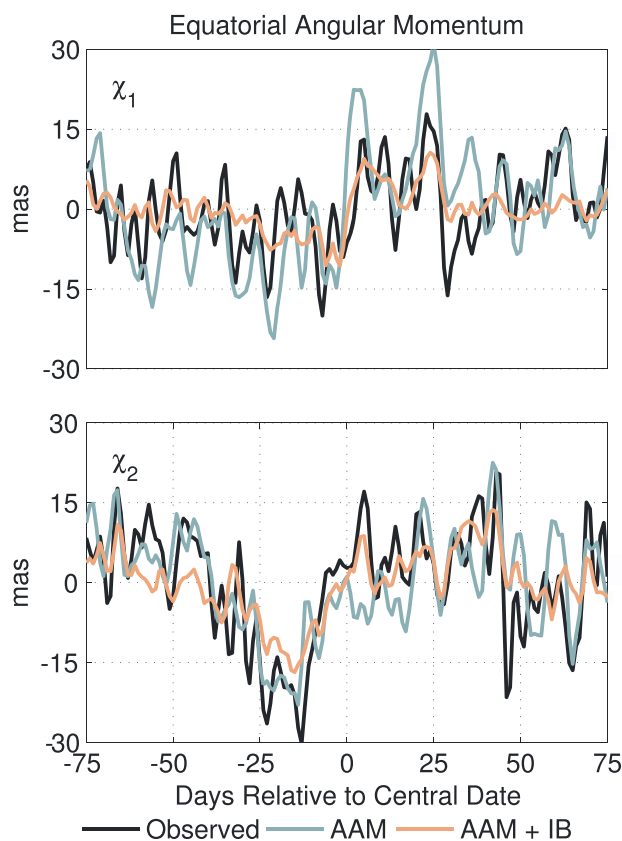


Figure 3. (top) Composites of the p_1 anomaly (black) and the corresponding AAM mass excitation function (χ_1^M), with and without the inverted barometer approximation (see text), composited over the 22 major warming events in ERA-Interim. (bottom) As for top row but for observed p_2 anomaly and corresponding components of the mass excitation function χ_2^M .

propagation, which intensifies in the month before the warming onset (Figures 4a and 4b).

The corresponding surface pressure anomaly (Figure 4d–4f), shows that the upward wave propagation is related, on average, to high-pressure anomalies over Eurasia and Northern Europe and low anomalies over the northeastern Pacific. *Garfinkel et al.* [2010] showed that, while the individual pressure anomalies preceding SSWs can vary greatly, SSWs are most efficiently induced by anomalies that project onto the climatological planetary wave 1 that results naturally from orographic and thermal forcing in the Northern Hemisphere. This means that SSWs are often associated with negative tropospheric geopotential height anomalies over the North Pacific and positive anomalies over Eastern Europe.

The meaning of this surface pressure pattern in terms of the AAM component χ_2^M is examined in Figures 4g–4i, which show the surface pressure anomalies weighted as in the integrand for the atmospheric moment of inertia (including the negative prefactor) in equation (6). The combined result of two surface pressure anomalies seen in Figure 4e is that χ_2^M becomes extremely negative in the month before the SSW onset.

The surface pressure signals preceding SSWs differ between vortex-displacement and vortex-splitting events, with vortex displacements more strongly associated with a low-pressure anomaly over North America, a high-pressure anomaly over Western Europe, and North Atlantic blocking, and vortex splits associated with high-pressure anomalies over the North Pacific and Siberia, a low-pressure anomaly over the North Atlantic, and North Pacific blocking with or without Atlantic blocking [*Martius et al.*, 2009; *Mitchell et al.*, 2012]. The surface anomaly pattern preceding vortex displacements is more closely associated with a wave 1 pressure anomaly (which would result in a negative χ_2^M anomaly), whereas vortex splits can be preceded by a wave 1 or wave 2 anomaly [*Bancalá et al.*, 2012; *Martius et al.*, 2009] (a wave 2 anomaly

function is shown by the orange curves, which agree much more with the observed polar motion in both cases. The strong variations of χ_1^M over the SSW life cycle are clearly damped out by the response of the ocean, leading to a much weaker observed variation in χ_1^{GEO} . This makes sense, since the weighting function for χ_1^M is maximal at 0° and 180°, i.e., over the oceans. χ_2^M , which happens to be weighted more strongly over the continents, clearly excites corresponding variations in χ_2^{GEO} . Therefore, the remainder of this paper will focus only on the angular momentum component χ_2^M .

4.2. Polar Motion Anomalies Preceding SSWs

Figure 4 examines the average surface pressure anomaly pattern associated with the SSWs at different points in time around the central date, along with the vertical profiles of geopotential height.

Figures 4a–4c show height-longitude slices of the geopotential height, averaged for each time block and over the 50°N–80°N latitudinal band. Geopotential height anomalies are computed with respect to the zonal mean and then scaled by the relative mass of each vertical layer in order to emphasize the tropospheric anomalies. The composite geopotential height anomalies extend with a westward tilt into the stratosphere, indicating upward planetary wave

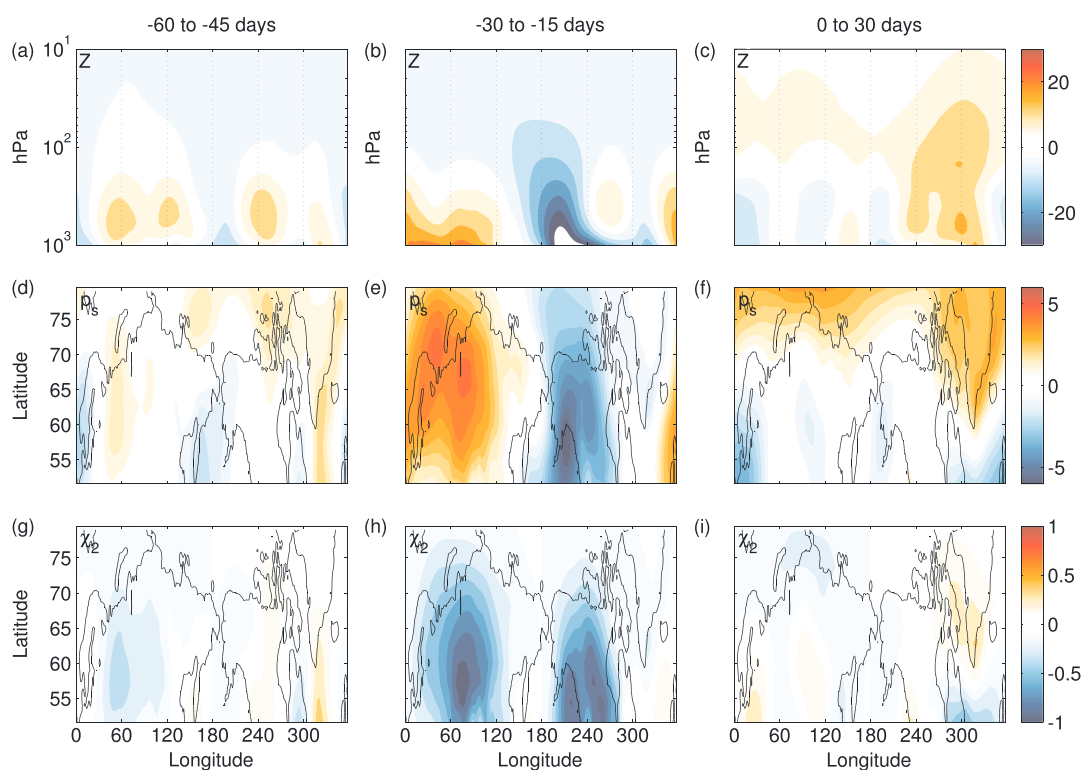


Figure 4. (a–c) Height-longitude cross sections of the geopotential height, composited over the 22 major warming events in ERA-Interim, averaged over three periods before and after the central date. (d–f) The corresponding composite surface pressure anomaly. (g–i) The surface pressure anomalies weighted by $\sin \phi \cos^2 \phi \sin \lambda$, as in the χ_2^M integral (equation (6)).

results in no net χ_2^M excitation), though this relationship seems to be strongly modulated by the phase of ENSO [Barriopedro and Calvo, 2014]. Compositing over splitting and displacement events separately, we found a slightly stronger χ_2^M anomaly for vortex displacement events but did not find the difference to vortex-splitting events to be statistically significant, presumably due to the relatively low sample size of each type of event and the overall diversity in precursors of both types of SSWs [Barriopedro and Calvo, 2014].

5. LOD Excitation by Wind Anomalies During SSWs

Returning back to the composite of all three ERPs over the SSW events (Figure 2), we see that SSWs on average do not just show a polar wobble but also a decline in ΔLOD (Figure 2e) starting roughly a month before the central date. This implies that the atmospheric precursors that give rise to SSW events also change the axial AAM.

The date at which ΔLOD begins to decline varies widely from event to event; for example, for the January 2009 event, the LOD decline begins about 50 days before the central date (Figure 1), while for the February 1979 event, it begins about 25 days before the central date. For the January 1987 event, a noticeable decline in LOD does not happen at all (not shown).

The average wind AEF (χ_3^W) is examined in Figure 5a, cast in terms of equivalent ΔLOD using (3) and compared to the observed ΔLOD . Variations of ΔLOD on this time scale are almost entirely explained by variations in the wind AEF, which is why the mass term (8), which is about an order of magnitude smaller [Eubanks et al., 1985], is omitted here.

We can investigate the source of the axial angular momentum anomaly more closely by decomposing it into contributions from different latitude bands. In Figure 5b, the global axial wind AEF (gray) is compared to the relative angular momentum of the following latitude bands: the south polar cap (SP, 90°S–60°S), southern midlatitudes (SH, 60°S–30°S), tropics (T, 30°S–30°N), northern midlatitudes (NH, 30°N–60°N), and the north polar cap (NP, 60°N–90°N).

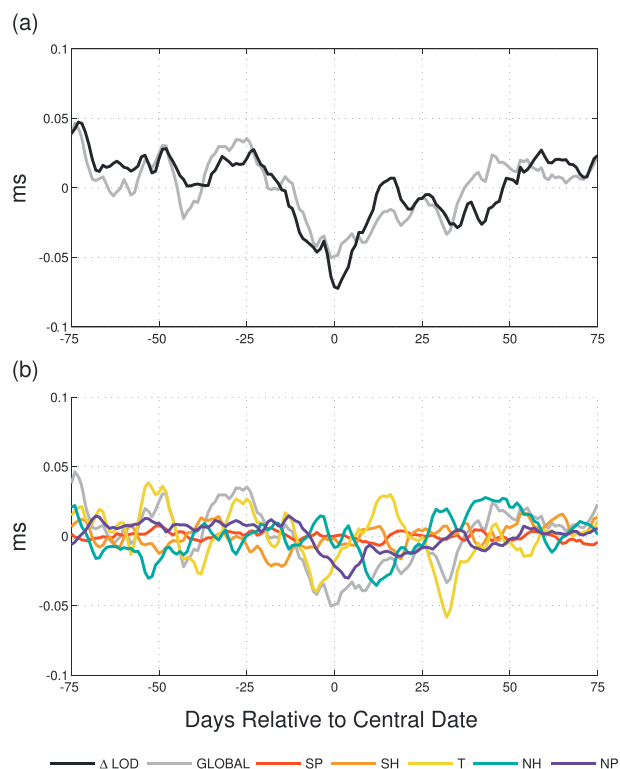


Figure 5. (a) The observed ΔLOD (black) and the corresponding axial wind excitation (χ_3^W , gray), composited over all major warming events in the joint data set. (b) The composite wind excitation functions integrated over different latitude bands, along with the global value (gray).

Here it can be seen that the wind reversal associated with the SSW causes a noticeable decline in relative angular momentum from the north polar band (dark blue), starting about 2 weeks before the central date. This angular momentum change contributes to the observed ΔLOD decline but does not account for all of it. We also see an angular momentum signal from the Northern Hemisphere extratropical band (green) that somewhat opposes the angular momentum from the polar band. The strongest contribution to the observed ΔLOD decline actually comes from the tropical band, which shows sharply decreasing angular momentum starting about 2 weeks before the central date and a positive anomaly after the central date. The prominence of the tropical band is not really surprising, since the tropics are most strongly weighted in the integral (equation (9)), but it is surprising that the tropical troposphere shows such strong angular momentum changes during SSWs.

The zonal mean zonal winds behind these angular momentum changes are shown in Figure 6 (left), averaged over four blocks of time around the central date that characterize the main ΔLOD changes: 60 to 20 days before the central date, when ΔLOD vacillates around 0; 15 days before to 15 days after the central date, when it reaches its observed minimum; 20 to 40 days after the central date, when it slowly recovers, and 40 to 60 days after the central date, when it has largely returned to zero anomalies.

We see that on average, the SSWs are associated with tropospheric zonal wind anomalies on the order of 1 m/s, which, though weak, is comparable to the response of tropospheric wind to temperature anomalies in the tropical lower stratosphere [Haigh et al., 2005]. Moreover, the contribution of these tropical wind anomalies to the axial AEF is stronger since lower levels of the atmosphere have exponentially more mass. To illustrate this, Figure 6 (right) shows pressure-latitude slices of daily anomalies of $u \cos^2 \phi dp$, i.e., the fractional axial angular momentum at each level. Here we see anomalous westerlies forming in the troposphere near the equator during the ± 15 days around the central date, which was also found by Kodera [2006] and attributed to the anomalous meridional circulation induced by the warming event at the poles.

The westerly anomalies would imply an increase in the ΔLOD , but are largely canceled out by easterly anomalies at higher latitudes. The real cause of the tropical contribution to the declining ΔLOD is that the northern side of the tropical band shows an easterly wind anomaly in the SSW precursor period (top row), which is then weakened as the central date is approached (second row). We also see tropical easterly wind anomalies intensifying in the 2 months after the central date, though these are partially canceled out by positive wind anomalies at midlatitudes.

Thus, it seems that SSWs are associated with tropical tropospheric wind anomalies throughout their life cycle, which are enough to cause a measurable decline in the observed ΔLOD . However, since the statistical significance of our composite ΔLOD signal is quite small, we defer a more thorough investigation of what causes these anomalies to future work.

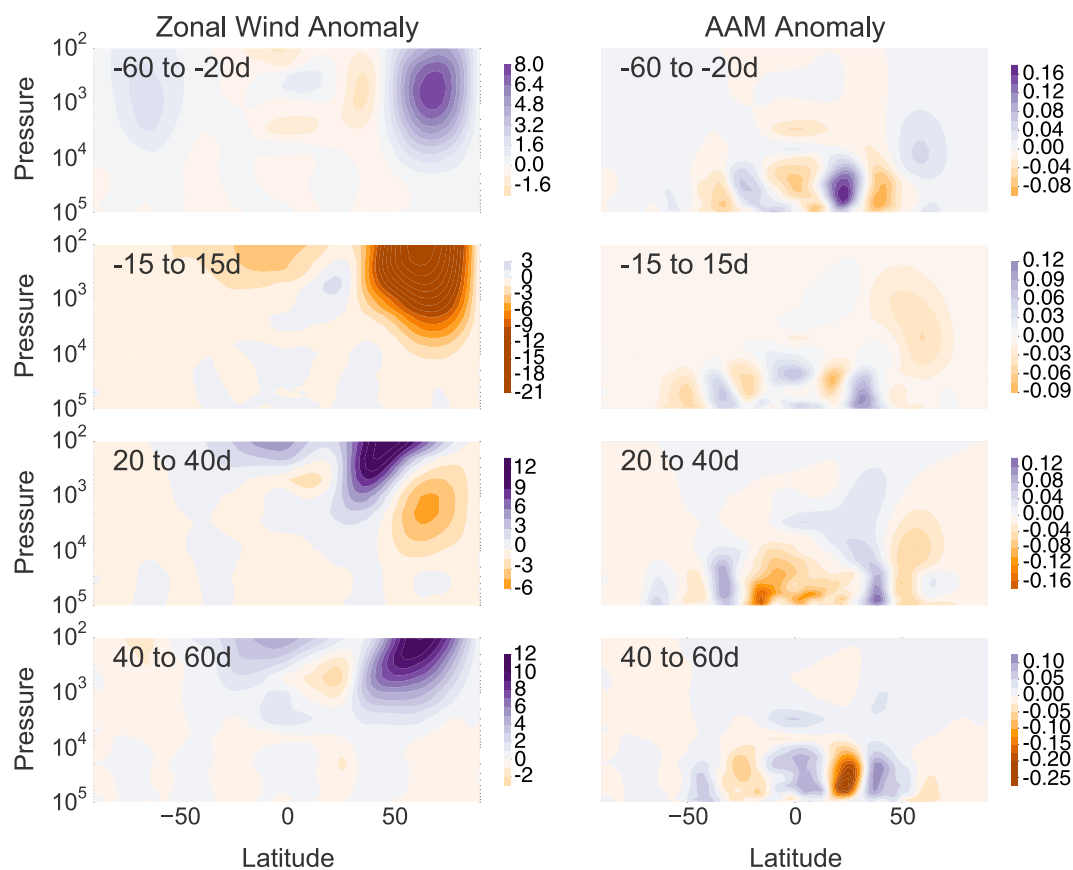


Figure 6. (left) Pressure-latitude slices of zonal mean zonal wind, averaged over four blocks of time around the central date (see text) and composited over all SSW events in the joint data set. (right) Multiplying the wind anomalies by $\cos^2 \phi$ and by the relative mass of each pressure level, such that each gridbox gives the local contribution to the global χ_3^M integral.

6. Summary and Conclusions

This study showed that sudden stratospheric warmings are often preceded by strong anomalies in the angular momentum of the atmosphere, which is observable as polar motion, and anomalies in the length of day. SSWs are typically preceded by strong anomalies in χ_2 , one of the two equatorial components of the atmospheric angular momentum, which fluctuates by about 30 mas over the life cycle of an SSW, showing a positive anomaly about 2 months before the 10 hPa wind reversal and a negative anomaly about 3 weeks before the wind reversal, though only the latter is statistically significant. For individual events (see supporting information) the total fluctuation of χ_2 can be as high as 60 mas. This is 4 times the observed annual polar wobble of about 15 mas [e.g. *Dobslaw et al., 2010*].

The cause of the negative χ_2 anomaly is the surface pressure pattern that is on average associated with planetary waves that eventually induce SSWs [*Garfinkel et al., 2010; Kodera et al., 2013*]: a positive pressure anomaly over Eurasia and an enhanced Aleutian or northeast Pacific low. As both surface pressure patterns contribute negatively to χ_2 , many SSWs are preceded by a negative χ_2 anomaly, even though they may not exhibit the full surface pressure anomaly pattern identified in Figure 4. A similar signal is not observed in χ_1 , the polar motion angle defined along the Greenwich Meridian, because the response of the oceans to atmospheric mass loading damps out the AAM anomalies in this direction.

Our work suggests that this polar wobble represents a new observable SSW precursor, which may aid in the prediction of SSWs, which is notoriously difficult. To investigate the efficacy of this signal as an observable precursor, Figures 7 and 8 show χ_2^{GEO} for all winters in the 1990s, which were relatively devoid of strong SSW events (Figure 7), and the 2000s, which exhibited several strong events (Figure 8). For each winter,

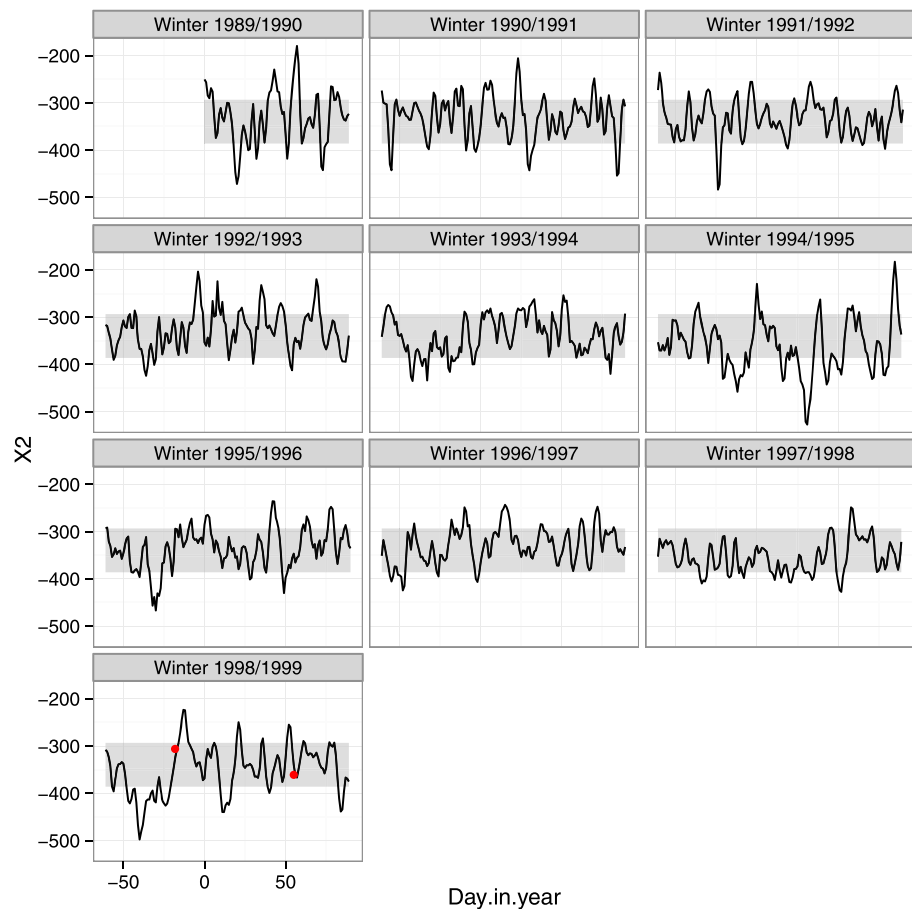


Figure 7. The χ_2^{GEO} for all 10 winters in the 1990s. The mean and standard deviation of χ_2^{GEO} over the period 1962–2010 are shown by the shaded band in each plot, and the central dates of the SSW events during this decade are shown by red dots.

the variation of χ_2^{GEO} is compared to the mean and standard deviation of χ_2^{GEO} over the entire epoch 1962–2010, and the central dates of SSW events are indicated by red dots.

It can be seen that strong negative anomalies in χ_2^{GEO} (i.e., anomalies outside of one standard deviation from the mean) are often harbingers of an SSW occurring 30–50 days later. All SSW events shown seem to be preceded by sharp negative values of χ_2^{GEO} in the month or two preceding the wind turnaround. On the other hand, extreme negative values of χ_2^{GEO} are also observed in winters without an SSW, including winters 1989/1990, 1991/1992, 1994/1995, and 1995/1996. A possible reason for this is that SSWs are not a simple response to tropospheric forcing but also depend on the condition of the stratosphere and whether planetary waves are able to propagate from the troposphere into the stratosphere.

SSWs may also be accompanied by a decline in the rate of the Earth’s rotation, or length of day, by a tenth of a millisecond on average (Figure 2e). For some warmings this effect is much stronger; for example, about a week before the central date the SSW event of February 2001 shows a ΔLOD of -0.6 ms, which is comparable to the 0.3–0.4 ms typically seen for subseasonal ΔLOD fluctuations [Eubanks et al., 1985; Rosen et al., 1991]. The decline in ΔLOD is the combined result of the stratospheric wind reversal from westerly to easterly, and westerly wind anomalies in the tropical troposphere, that may precede an SSW and then decline at the onset of the event. However, it is difficult to say whether this is a statistically significant result.

We did not find statistically significant differences in compositing between vortex-splitting or displacement events in either the χ_2 or ΔLOD anomalies, even though previous studies have shown significant differences in the precursor anomaly patterns associated with vortex splits and displacements [Martius et al., 2009; Mitchell et al., 2012]. The difference in the Earth rotation signature of these types of events and a possible

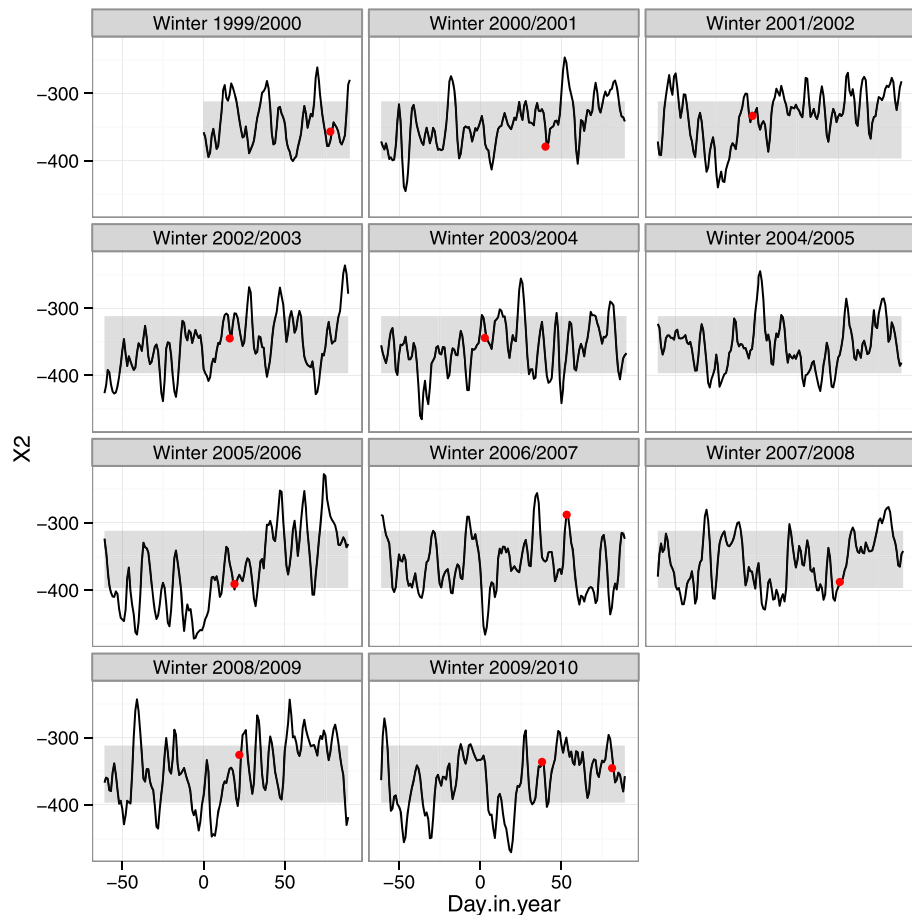


Figure 8. As in Figure 7 but for the first decade of the 2000s.

modulation of this relationship by ENSO [Barriopedro and Calvo, 2014] would be interesting to investigate in the future when more data are available.

Note also that this study has not discussed the transfer of AAM to the solid Earth, which typically happens by a combination of torques from surface friction and pressure systems around mountains [Egger *et al.*, 2007]. Since the estimated AAM explains most of the observed Earth rotation changes during SSWs, it is not necessary for the purpose of this study to estimate individual torques. However, a calculation of the relative magnitudes of the different torques would be an interesting point of future research.

Acknowledgments

This work has been performed within the Helmholtz-University Young Investigators Group NATHAN, funded by the Helmholtz Association through the President’s Initiative and Networking Fund, the Helmholtz Centre for Ocean Sciences Kiel, the Helmholtz Centre for Geosciences Potsdam, and the Freie Universität Berlin. We are grateful to Nour-Eddine Omrani for helpful discussions and to Christian Blume for help with the SSW selection algorithm. For information on how to obtain the data used to produce the results of this paper, please contact Dr. L. Neef.

References

Ayarzagüena, B., U. Langematz, and E. Serrano (2011), Tropospheric forcing of the stratosphere: A comparative study of the two different major stratospheric warmings in 2009 and 2010, *J. Geophys. Res.*, *116*, D18114, doi:10.1029/2010JD015023.

Baldwin, M. P., and T. J. Dunkerton (2001), Stratospheric harbingers of anomalous weather regimes, *Science*, *294*, 581–584.

Bançalá, S., K. Krüger, and M. Giorgetta (2012), The preconditioning of major sudden stratospheric warmings, *J. Geophys. Res.*, *117*, D04101, doi:10.1029/2011JD016769.

Barnes, R., R. Hide, A. White, and C. Wilson (1983), Atmospheric angular momentum fluctuations, length-of-day changes and polar motion, *Proc. R. Soc. London, Ser. A*, *387*, 31–73.

Barriopedro, D., and N. Calvo (2014), On the relationship between ENSO, stratospheric sudden warmings, and blocking, *J. Clim.*, *27*, 4704–4720.

Chao, B., and A. Y. Au (1991), Atmospheric excitation of the Earth’s annual wobble: 1980–1988, *J. Geophys. Res.*, *96*(B4), 6577–6582.

Charlton, A. J., and L. M. Polvani (2007), A new look at stratospheric sudden warmings. Part I: Climatology and modeling benchmarks, *J. Clim.*, *20*, 449–469.

Dee, D. P., et al. (2011), The ERA-Interim reanalysis: Configuration and performance of the data assimilation system, *Q. J. R. Meteorol. Soc.*, *137*(656), 553–597, doi:10.1002/qj.828.

Dobslaw, H., R. Dill, A. Grötsch, A. Brzezinski, and M. Thomas (2010), Seasonal polar motion excitation from numerical models of atmosphere, ocean, and continental hydrosphere, *J. Geophys. Res.*, *115*, B10406, doi:10.1029/2009JB007127.

Egger, J., K. Weickmann, and K.-P. Hoinka (2007), Angular momentum in the global atmospheric circulation, *Rev. Geophys.*, *45*, RG4007, doi:10.1029/2006RG000213.

- Eubanks, T., J. Steppe, J. Dickey, and P. Callahan (1985), A spectral analysis of the Earth's angular momentum budget, *J. Geophys. Res.*, *90*, 5385–5404.
- Eubanks, T., J. Steppe, J. Dickey, R. Rosen, and D. Salstein (1988), Causes of rapid motions of the Earth's pole, *Nature*, *334*, 115–119.
- Garfinkel, C. I., and D. L. Hartmann (2008), Different ENSO teleconnections and their effects on the stratospheric polar vortex, *J. Geophys. Res.*, *113*, D18114, doi:10.1029/2008JD009920.
- Garfinkel, C. I., D. L. Hartmann, and F. Sassi (2010), Tropospheric precursors of anomalous Northern Hemisphere stratospheric polar vortices, *J. Clim.*, *23*(12), 3282–3299, doi:10.1175/2010JCLI3010.1.
- Gross, R. S. (1992), Correspondence between theory and observations of polar motion, *Geophys. J. Int.*, *109*, 162–170.
- Gross, R. S. (2009), Earth rotation variations—Long period, in *Geodesy, Treatise on Geophysics*, edited by R. S. Gross, pp. 239–294, Elsevier, Amsterdam, Netherland.
- Haigh, J. D., M. Blackburn, and R. Day (2005), The response of tropospheric circulation to perturbations in lower-stratospheric temperature, *J. Clim.*, *18*, 3672–3685.
- Harada, Y., A. Goto, H. Hasegawa, and N. Fujikawa (2009), A major stratospheric sudden warming event in January 2009, *J. Atmos. Sci.*, *67*, 2052–2069.
- Hide, R., J. Dickey, S. Marcus, R. Rosen, and D. Salstein (1997), Atmospheric angular momentum fluctuations during 1979–1988 simulated by global circulation models, *J. Geophys. Res.*, *102*, 16,423–16,438.
- Kodera, K. (2006), Influence of stratospheric sudden warming on the equatorial troposphere, *Geophys. Res. Lett.*, *33*, L06804, doi:10.1029/2005GL024510.
- Kodera, K., N. Eguchi, J. N. Lee, Y. Kuroda, and S. Yukimoto (2011), Sudden change in the tropical stratosphere and troposphere during January 2009, *J. Meteorol. Soc. Jpn.*, *89*, 283–290, doi:10.2151/jmsj.2011-208.
- Kodera, K., H. Mukougawa, and A. Fujii (2013), Influence of the vertical and zonal propagation of stratospheric planetary waves on tropospheric blockings, *J. Geophys. Res. Atmos.*, *118*(15), 8333–8345, doi:10.1002/jgrd.50650.
- Labitzke, K., and B. Naujokat (2000), On the remarkable arctic winter in 2008/2009, *SPARC Newsl.*, *15*, 11–14.
- Labitzke, K., and B. Naujokat (2009), On the remarkable arctic winter in 2008/2009, *J. Geophys. Res.*, *114*, D00102, doi:10.1029/2009JD012273.
- Martius, O., L. Polvani, and H. Davies (2009), Blocking precursors to stratospheric sudden warming events, *Geophys. Res. Lett.*, *36*, L14806, doi:10.1029/2009GL038776.
- Mitchell, D. M., L. J. Gray, J. Anstey, M. P. Baldwin, and A. J. Charlton-Perez (2012), The influence of stratospheric vortex displacements and splits on surface climate, *J. Clim.*, *26*, 2668–2682, doi:10.1175/JCLI-D-12-00030.1.
- Nastula, J., D. Salstein, and B. Kolczek (2009), Patterns of atmospheric excitation functions of polar motion from high-resolution regional sectors, *J. Geophys. Res.*, *114*, B04407, doi:10.1029/2008JB005605.
- Quiroz, R. S. (1986), The association of stratospheric warmings with tropospheric blocking, *J. Geophys. Res.*, *91*(D4), 5277–5285.
- Rosen, R. D., and D. A. Salstein (1983), Variations in atmospheric angular momentum on global and regional scales and the length of day, *J. Geophys. Res.*, *88*, 5451–5470.
- Rosen, R. D., and D. A. Salstein (1985), Contribution of stratospheric winds to annual and semiannual fluctuations in atmospheric angular momentum and the length of day, *J. Geophys. Res.*, *90*, 8033–8041.
- Rosen, R. D., D. A. Salstein, and T. M. Wood (1990), Discrepancies in the Earth-atmosphere angular momentum budget, *J. Geophys. Res.*, *95*(89), 265–279.
- Rosen, R. D., D. A. Salstein, and T. M. Wood (1991), Zonal contributions to global momentum variations on intraseasonal through interannual timescales, *J. Geophys. Res.*, *96*, 5145–5151.
- Salstein, D. A., and R. D. Rosen (1989), Regional contributions to the atmospheric excitations of rapid polar motions, *J. Geophys. Res.*, *94*, 9971–9978.
- Thompson, D. W., M. P. Baldwin, and J. M. Wallace (2002), Stratospheric connection to Northern Hemisphere wintertime weather: Implications for prediction, *J. Clim.*, *15*, 1421–1428.
- Uppala, S. M., et al. (2005), The ERA-40 Re-analysis, *Q. J. R. Meteorol. Soc.*, *131*(612), 2961–3012, doi:10.1256/qj.04.176.
- Wilks, D. S. (1995), *Statistical Methods in the Atmospheric Sciences: An Introduction*, 467 pp., Academic Press, San Diego, Calif.
- Woollings, T., A. Charlton-Perez, S. Ineson, A. Marshall, and G. Masato (2010), Associations between stratospheric variability and tropospheric blocking, *J. Geophys. Res.*, *115*, D06108, doi:10.1029/2009JD012742.
- Wunsch, C., and D. Stammer (1997), Atmospheric loading and the oceanic “inverted barometer” effect, *Rev. Geophys.*, *35*(1), 79–107.
- Zhou, Y., J. Chen, and D. Salstein (2008), Tropospheric and stratospheric wind contributions to Earth's variable rotation from NCEP/NCAR reanalyses (2000–2005), *Geophys. J. Int.*, *174*, 453–463, doi:10.1111/j.1365-246X.2008.03843.